

# TROPICAL–TEMPERATE LINKS IN SOUTHERN AFRICAN AND SOUTHWEST INDIAN OCEAN SATELLITE-DERIVED DAILY RAINFALL

RICHARD WASHINGTON\* and MARTIN TODD

*School of Geography, University of Oxford, Oxford, OX1 3TB, UK*

*Received 1 August 1997*

*Revised 10 December 1998*

*Accepted 15 December 1998*

## ABSTRACT

An objective analysis of daily austral summer rainfall variability in the southern Africa and Southwest Indian Ocean region, using satellite-derived rainfall estimates, is conducted for the first time. A new method to reconstruct the GOES Precipitation Index (GPI), at the daily scale on a 2.5° grid, from ISCCP D1 satellite products is introduced. Estimates using this method are validated with GPI estimates on a monthly scale over global and regional domains. The reconstructed GPI (RGPI) estimates correlate very strongly with those from the GPI. Empirical Orthogonal Function (EOF) analysis of RGPI daily rainfall estimates for November–March (15–40°S, 10–70°E) shows that the leading mode of variability is characterised by tropical–temperate links in all months. These rain bands are orientated from north-west to south-east across the study region. Events characteristic of the leading mode of variability are relatively infrequent, occurring on average only twice per month, and can be stationary or propagating systems. A rainfall dipole exists, with parallel centres of activity producing enhanced (suppressed) activity over the Southwest Indian Ocean, associated with suppressed (enhanced) activity over southern Africa. Previous studies have shown that this dipole exists at monthly and interannual scales. This rainfall dipole has tropical–temperate links, whereas previous land-based rainfall analyses have emphasised only the tropical and subtropical components. Copyright © 1999 Royal Meteorological Society.

KEY WORDS: daily rainfall; southern Africa; Southwest Indian Ocean; tropical–temperate links; satellite; ISCCP; infrared; empirical orthogonal functions

## 1. INTRODUCTION

Tropical–temperate interactions in the atmosphere form an intriguing element of the general circulation, not least because theory has grown predominantly around either the tropics or the temperate latitudes, thereby rendering such cross-latitudinal links scientific itinerants of the core discipline. Southern Africa and the Southwest Indian Ocean has, for some time, been identified as an important location for tropical–temperate interactions.

Harangozo and Harrison (1983), Harrison (1984a,b,c), Smith (1985) and Diab *et al.* (1991) have all shown that troughs linking tropical convection over southern Africa, with transients in the zonal westerlies, identifiable as cloud bands on visible and infrared satellite imagery, are an important summertime rainfall-producing system over the southern African subcontinent. Further work on extreme rainfall events (Walker and Lindesay, 1989; Lindesay and Jury, 1991) have similarly implicated these systems.

Efforts to explain the high degree of rainfall variability in southern Africa have led to the development of conceptual models of wet- and dry-spells in southern Africa (Tyson, 1986). Such models feature the relocation of cloud bands linking tropical and temperate rainfall, from the subcontinent, where they are

\* Correspondence to: School of Geography, University of Oxford, OX1 3TB, UK;  
e-mail: Richard.Washington@geography.ox.ac.uk

found during wet conditions, to the Southwest Indian Ocean, and in dry summer to over southern Africa. These conceptual models have been used to infer climates of the last glacial maximum (Cockcroft *et al.*, 1987), the late Holocene (Tyson and Lindesay, 1992; Cohen and Tyson, 1995) and those of the next century (Tyson, 1993). The importance of these tropical–temperate links is thus beyond question.

Despite this, an objective analysis of the spatial structure of daily rainfall over southern Africa and the Southwest Indian Ocean still remains to be done. The most comprehensive work has been undertaken by Harrison (1984a,b,c), who defined an objective classification scheme of southern African summer (September–April) rainfall, based on Principal Component Analysis (PCA) of 64 rainfall districts. In his pioneering work, the identification of the rain-bearing synoptic systems, surmised to be represented on each principal component, were deduced from the inspection of polar-orbiting satellite imagery using the principal component scores to indicate months of high or low activity. Ultimately the link from individual synoptic systems to the monthly rainfall classification is thus subjective. The study was confined to rainfall over land areas, with the relocation of cloud bands to the Southwest Indian Ocean during dry years in southern Africa inferred from subsequent inspection of satellite imagery. Similarly the work of Diab *et al.* (1991), although explicitly including upper air data, remained subjective in linking daily rainfall with a discriminant analysis-based classification of synoptic systems. In this sense, an objective and direct link between daily rainfall and the cloud bands spanning tropical–temperate troughs has not been achieved.

With the benefit of recently released daily satellite-derived products, the authors aim to identify objectively and directly the structure of daily land and ocean rainfall during individual months for the southern African and Southwest Indian Ocean region. The algorithm used to generate daily rainfall, including data verification, is detailed in section 2. Empirical Orthogonal Functions (EOFs) are used to develop an objective pattern of daily rainfall variability. The details of this are found in section 3 and the results in section 4. The implications are discussed in the closing section.

## 2. DAILY SATELLITE RAINFALL DATA

### 2.1. Data

Over much of the globe, information on daily rainfall is most accurately obtained from geostationary satellite infrared data. Passive microwave satellite data has a more direct link with rainfall, but the temporal sampling of current systems is inadequate for accurate estimates of daily rainfall (Barrett and Beaumont, 1994). Other studies (Nogues-Paegle and Mo, 1997) have used outgoing long-wave radiation (OLR) data from NOAA polar-orbiting satellites as a proxy for rainfall. This is based on an average of single morning and evening passes of the satellite. Geostationary data provides much-improved temporal resolution, resulting in reduced errors. Morrissey and Janowiak (1996) show that for pentad and monthly estimates of tropical rainfall, temporal subsampling-associated satellite estimation introduces a conditional bias where the algorithm overestimates high rainfall and underestimates low rainfall. The magnitude of this conditional bias is dependent on a number of factors, including sampling rate, integration area and study region. For a 3-hourly sampling scheme the conditional bias is very close to zero but increases markedly for a 12-hourly scheme. Li *et al.* (1996) assessed the errors in estimation of monthly rainfall associated with a variety of sampling schemes using data from the Darwin (Australia) rain radar. It is shown that estimates are sensitive not only to the rate of sampling, but to the starting time of the scheme, due to the diurnal cycle of rainfall. Again, a 3-hourly scheme shows minimal bias in comparison to a 12-hourly scheme, where bias ranged from +20 to –20% depending on sampling starting time. Soman *et al.* (1995) produced very similar results using the Darwin radar data from two 20-day periods. From these studies it appears that sampling errors will be greater over land, where the diurnal cycle is more pronounced. There has been no assessment of our knowledge concerning the errors in daily estimates of rainfall associated with temporal sampling.

The limitations of any single sensor to accurately estimate rainfall has recently led to a number of merged rainfall products which utilise data from multiple sources, such as geostationary IR satellite data, passive microwave satellite data, rain gauge observations and numerical models analysis fields (Huffman *et al.*, 1997; Xie and Arkin, 1997). Such products are as yet only available with a minimum of monthly temporal resolution.

In this study, data from the International Satellite Cloud Climatology Program (ISCCP, Schiffer and Rossow, 1985) is obtained from the Langley Distributed Active Archive Centre. ISCCP data is available in a number of formats. The D1 format provides global estimates of cloud characteristics on a 2.5° latitude-longitude grid for the periods listed in Table I at a 3-hourly interval (Rossow and Schiffer, 1991; Rossow *et al.*, 1996). In the tropical regions, this is based primarily on data from four geostationary satellites (GOES-E, GOES-W, Meteosat and GMS). The absence of data from the Indian Geostationary Satellite (INSAT) for some of the study period results in poor geostationary coverage over the Indian Ocean between 50–90°E. In this region, cloud characteristics are derived from the NOAA polar-orbiting satellites with consequently reduced temporal resolution. As the ISCCP program is as yet incomplete, the data used only represents a subset of that which will eventually become available.

## 2.2. Reconstruction of GOES Precipitation Index rainfall estimates from ISCCP D1 data

The GOES Precipitation Index (GPI, Arkin and Meisner, 1987; Arkin *et al.*, 1994) is the most widely used and thoroughly evaluated satellite rainfall-estimation technique. Whilst estimates based on infrared satellite observations suffer from the relatively indirect relationship between cloud top temperature and rainfall, this problem is minimised in tropical regions where convective rainfall systems dominate. In addition, the use of geostationary satellite data effectively eliminates bias associated with diurnal rainfall cycles. However, extensive validation of the GPI has suggested that whilst the GPI produces a small bias over the tropical and subtropical oceans, estimates over land are greater than those from conventional measurements (Kidd and Adler, 1997). Given that the GPI was calibrated using data from the Global Atmospheric Research program (GARP), and from the Global Atlantic Tropical Experiment (GATE), it is likely that some regional recalibration would result in improved accuracy. Using the GPI, rainfall is calculated from:

$$R = F_c GT \quad (1)$$

where  $F_c$  is the fractional coverage of each 2.5° cell by cloud colder than 235 K,  $G$  is the GPI coefficient equal to 3.0, and  $T$  is the number of hours in the integration period.

Daily global GPI data are not available from any known source. In this study, daily rainfall estimates are derived using a reconstructed GPI, derived from 3-hourly ISCCP D1 data using the method described by Todd and Washington (1998). The ISCCP D1 data retains the first and second moments of the distribution of cloud top temperatures, as well as the number of satellite observations within each 2.5° cell. From probability theory, assuming a normal distribution, the fractional coverage of observations below the GPI threshold of 235 K within each 2.5° cell is estimated. Daily rainfall,  $R$  is then calculated from the standard GPI equation (1). Finally, to account for non-normal distributions, a correction is employed, based on the mean cloud top temperature.

Table I. Months and years of daily data used in the analysis

November	December	January	February	March
1986	1986	1986	1986	1986
1989	1989	1987	1990	1990
1990	1990	1990	1991	1991
1991	1991	1991	1992	1992
1992	1992	1992	1993	1994
		1993		

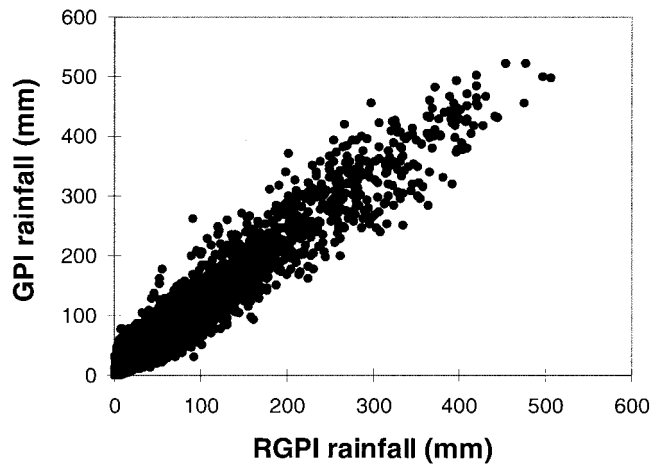


Figure 1. Relationship between monthly rainfall estimates over study domain from GPI and RGPI methods from data from the months and years listed in Table I

Variable satellite–Earth geometry is believed to result in systematic bias of rainfall estimates, particularly towards the edge of the Earth disk viewed by a geostationary satellite as the viewing angle becomes increasingly oblique (Joyce and Arkin, 1997). The RGPI estimates contain a correction,  $Z_{sc}$ , to account for this:

$$\text{RGPI} = R \times Z_{sc} \quad (2)$$

$$Z_{sc} = a + (z \times b) \quad (3)$$

where  $z$  is the satellite zenith angle and  $a$  and  $b$  are empirically-derived constants, equal to 1.22891 and  $-0.009028$ , respectively, obtained from the study by Joyce and Arkin (1997).

Daily rainfall anomalies (RGPI<sub>a</sub>) are calculated from:

$$\text{RGPI}_{ai} = \text{RGPI}_i - \text{GPI}_m \quad (4)$$

where  $\text{RGPI}_i$  is the daily RGPI value for a given grid cell and  $\text{GPI}_m$  is the unconditional daily rain rate for the appropriate month.  $\text{GPI}_m$  is derived for each month from the 11-year database of monthly GPI estimates (Janowiak and Arkin, 1991) covering the period January 1986–September 1996, obtained from the Climate Analysis Centre of NOAA. Thus daily rainfall anomalies are produced at  $2.5^\circ$  resolution for the months listed in Table I.

Todd and Washington (1998) show that the RGPI estimates rainfall composited over monthly and pentad periods correlate very strongly with the GPI and have minimal bias, irrespective of the integration period selected or the underlying surface type (Figure 1, Table II). Comparison with the independent NASA WetNet PIP-3 surface-rainfall validation data shows that the RGPI estimates match the validation data with accuracy very similar to that of the GPI and are comparable to many passive microwave algorithms. Both the RGPI and GPI estimates of rainfall match the validation data more closely over the tropical Pacific Ocean than over the tropical and subtropical land masses, where a positive bias is apparent.

Table II. Validation statistics (correlation and bias) for RGPI tropical rainfall estimates versus GPI estimates

Validation domain	RGPI mean bias	Correlation coefficient
Global tropics 40°N–40°S	–1%	0.97
Study domain 15–40°S, 7.5–70°E	–2%	0.97

### 3. METHODS OF ANALYSIS

The analysis of rainfall in the southern African-Southwest Indian Ocean region was undertaken for a number of domains. These are discussed below. Since the intention of this study is to determine objectively the spatial extent and temporal characteristics of leading modes of daily rainfall variability in the southern Africa-Southwest Indian Ocean region, EOFs of daily rainfall with space as variables and time as observations, were calculated for individual months of November-March.

The literature on EOF analysis is extensive (Richman, 1986; Joliffe, 1987; White *et al.*, 1991). A major documented problem with this method is that unrotated EOFs have a tendency to produce predictable patterns. The first component maximises the explained variance by having generally large loadings on all variables, and subsequent patterns are dipoles or more complex patterns. Buell (1975), for example, warns that unrotated EOFs may not capture the nature of the well known correlation functions. Their direct interpretation can thus be misleading. Rotation of the EOFs is regarded as one possible solution to this (Richman, 1986).

Eigenvectors may also be extracted from either the covariance or the correlation matrix  $\mathbf{S}$  of  $j \times j$  variables. Where the variables,  $j$ , correspond to some field for which the true size of the variability is deemed important (such as sea surface temperatures), the covariance matrix is applicable (Folland *et al.*, in press). If the variability across the variables  $j$  is large, but unimportant in the sense that identification of simultaneous spatial variability across all variables  $j$  through time  $i$  is the aim of the analysis, then the correlation matrix is applicable as the input to the EOF calculation. Rainfall varies extensively across a broad subtropical domain such as the one being assessed here. Since the authors wish to assess modes of variability which may be connected across regions of quite different rainfall climatologies, it is reasonable to use the correlation matrix as an input to the EOF analysis.

Given these concerns, a number of experiments were nevertheless undertaken so that the EOF solutions presented are not contingent upon *a priori* decisions. Unrotated and Varimax-rotated eigenvectors of the rainfall grid box covariance and correlation matrix were all calculated. In addition, the domain was altered to include: (i) land areas only between 15 and 35°S; (ii) land and sea between 15 and 40°S and from 7.5 to 50°E; (iii) land and sea between 15 and 40°S and from 7.5 to 70°E. A total of 12 suites of experiments were undertaken (which include all the combinations of the above) for each of the months November-March, yielding 60 suites of EOFs.

Only the unrotated eigenvectors of the correlation matrix for the domain 15-40°S and 7.5-70°E (domain c) are presented. Varimax rotation had the effect of over-regionalising the EOFs so that as few as two or three grid boxes contained high loadings. This is likely to be a result of the domain/spatial resolution ratio being excessively small. Further, the leading unrotated EOF, in all months except February, emerged as a dipole pattern rather than centred, positive, uniform loadings suggested by Buell (1975). The authors will argue that the leading unrotated EOFs have a physical meaning. The modulus of covariance eigenvectors weights over the land and sea domains (b and c above) were typically large in the tropical regions only, reflecting the higher rainfall rates associated with tropical convection. Since the correlation matrix effectively standardises rainfall across the domain, thereby giving equal weighting to all grid boxes in the study, interactions between regions of differing total rainfall could be identified, while not falsely including hyper-arid regions of southwest Africa and the adjacent Atlantic Ocean. EOFs calculated over the two large domains incorporating land and sea (domains b and c) were very similar. The larger domain is preferred, as the smaller (domain b) curtails some of the high loadings on the eastern edge. Hence EOFs of the unrotated correlation matrix of daily rainfall over the domain 15-40°S, 10-70°E are retained for discussion.

Sensitivity of the EOFs to rainfall spatial resolution has been assessed for the set of EOFs presented here. This is an important step, given the relatively short length of the data and the possible instability of the data matrix. The data were interpolated to a  $5 \times 5^\circ$  and also  $5 \times 10^\circ$  latitude-longitude grid and the EOFs recalculated over three resolutions. The leading EOFs for all months, except January, are insensitive to these changes in spatial resolution. This was determined as follows: leading eigenvectors for each of the 5 months, calculated at three resolutions ( $2.5 \times 2.5^\circ$ ,  $5 \times 5^\circ$ ,  $5 \times 10^\circ$  latitude-longitude), were

Table III. Variance of monthly EOFs and sampling errors based on North Test (North *et al.*, 1982). / = Pass, x = fail

EOF	Nov Var	North, <i>n</i> = 150	Dec Var	North, <i>n</i> = 155	Jan Var	North, <i>n</i> = 186	Feb Var	North, <i>n</i> = 141	Mar Var	North, <i>n</i> = 155
1	8.54	0.34 /	9.41	0.35 /	8.11	0.30 x	8.37	0.34 /	7.60	0.31 /
2	6.78	0.21 /	7.93	0.32 /	7.86	0.29 /	6.52	0.30 /	6.83	0.30 /
3	5.84	0.28 /	5.46	0.27 /	5.28	0.24 /	5.42	0.28 /	5.72	0.27 /
4	5.11	0.26 /	5.00	0.25 x	4.43	0.02 /	4.52	0.25 /	4.81	0.25 /
5	4.67		4.80		4.00		4.10		4.26	

interpolated to a common grid ( $5 \times 10^\circ$ ) and correlated with each other. In all months except January, the correlations (not shown) between the leading eigenvectors calculated at the three spatial resolutions significant at the 99% level. Reasons for the sensitivity of January are explored in section 4.

Time coefficients (scores) of the EOFs, given by the cross product of the eigenvectors and the standardised daily rainfall time series, have also been computed to allow interpretation of the temporal variability of the leading modes.

#### 4. RESULTS

The eigenvalue proportions of the first five EOFs are shown in Table III. The stability of the EOFs has been determined using the North Test (North *et al.*, 1982) which is based on an estimate of the sampling errors of each eigenvalue. All leading EOFs are distinct, except for January, where EOF1 and EOF2 are confounded. An alternative approach to identifying those eigenvalues in noise-subspace, using Monte Carlo simulations, is based on the random exclusion of five observations (corresponding to 5 days) from the rainfall data before calculating the EOFs. This randomisation process is repeated 200 times. Overlap between EOFs is determined by the standard deviation of the eigenvalues. All months, including January, emerge with distinct leading EOFs if this method is used. It is likely that the confounding of EOF 1 and 2 in January (based on the North Test) results from the inclusion of certain critical days in the January daily rainfall record. Discussion returns to this possibility later.

The leading EOFs of daily rainfall for individual months from November to March are shown in Figure 2(a)–(f). The eigenvectors are shown as the correlation coefficients between the daily rainfall time series at each of the  $2.5 \times 2.5^\circ$  grid boxes and the EOF time coefficients (scores).

Each of the months studied features a loading field pattern which links tropical convective rainfall with rainfall derived from disturbances in the temperate latitudes. In the November the tropical–temperate band is orientated from north-west to south-east across the eastern half of tropical southern Africa (including Zambia, Mozambique and Malawi) towards the extreme Southwest Indian Ocean (Figure 2(a)). Near-uniform loadings indicate that the feature is physically continuous, with components north of the domain boundary. Weaker negative loadings, indicating the presence of a weak dipole, extend in a similar orientation across Namibia, Botswana and South Africa. Figure 3(a) shows an example of the leading November mode. Rainfall anomalies peak above  $20 \text{ mm day}^{-1}$  in the southern-most extent of the domain while anomalies greater than  $10 \text{ mm day}^{-1}$  within the core of the band, cover some  $20^\circ$  in latitude.

The leading EOF in December (Figure 2(b)) depicts a similar pattern, except that the main tropical–temperate band is shifted about  $12^\circ$  east, so that convection on the Mozambique coast links with rainfall in the Southwest Indian Ocean near  $25^\circ\text{S}$ ,  $50^\circ\text{E}$ . In contrast to November, the loadings are highest over the ocean. A weaker band of negative loadings, orientated meridionally, with an axis some  $25\text{--}30^\circ$  west of the main band, is centred over the southern African subcontinent. An event typical of this mode in December is shown in Figure 3(b).

The situation in January (Figure 2(c)) is almost identical to that of December, except that the modulus of the loadings is similar in the two parallel bands, possibly as a result of enhanced land-based convection

associated with the annual march of rainfall. Since the leading January EOF fails the North Test, the second EOF for this month (Figure 2(d)) is also considered. This EOF also shows a tropical-temperate rainfall link, with an orientation similar to that of the leading November EOF. Overlap in the sampling errors in January is likely to result from the physical proximity between the rain bands in EOF1 and EOF2. The fact that the Monte Carlo approach to determining the sampling errors indicated that these EOFs are distinct, suggests that a low number of episodes, or possibly a slowly-propagating system may have determined the structure of this EOF. When calculated over the coarser resolutions, EOF1 and EOF2 merge, again suggesting that the fine resolution has captured a similar physical feature, but in a slightly different phase.

A representative event of January EOF1 (12 January, 1993) is shown in Figure 3(c). On this day the largest rainfall anomalies ( $> 25 \text{ mm day}^{-1}$ ) were located over tropical central-east Africa, but a broad band of rainfall anomalies near  $15 \text{ mm day}^{-1}$  extended south-eastward to link with temperate rainfall.

The leading EOFs of November, December and January daily rainfall have all been characterised by two tropical-temperate rain bands of opposite sign orientated north-west to south-east with axes over the subcontinent and the Southwest Indian Ocean. February is unique in that a single tropical-temperate rain-band links south-eastern southern Africa with the Southwest Indian Ocean. Instead of the land-based convection centred over southern Africa linking with temperate rainfall systems, convection over Zambia, Zimbabwe and Western Angola links with convection over the sub-tropical Indian Ocean and the

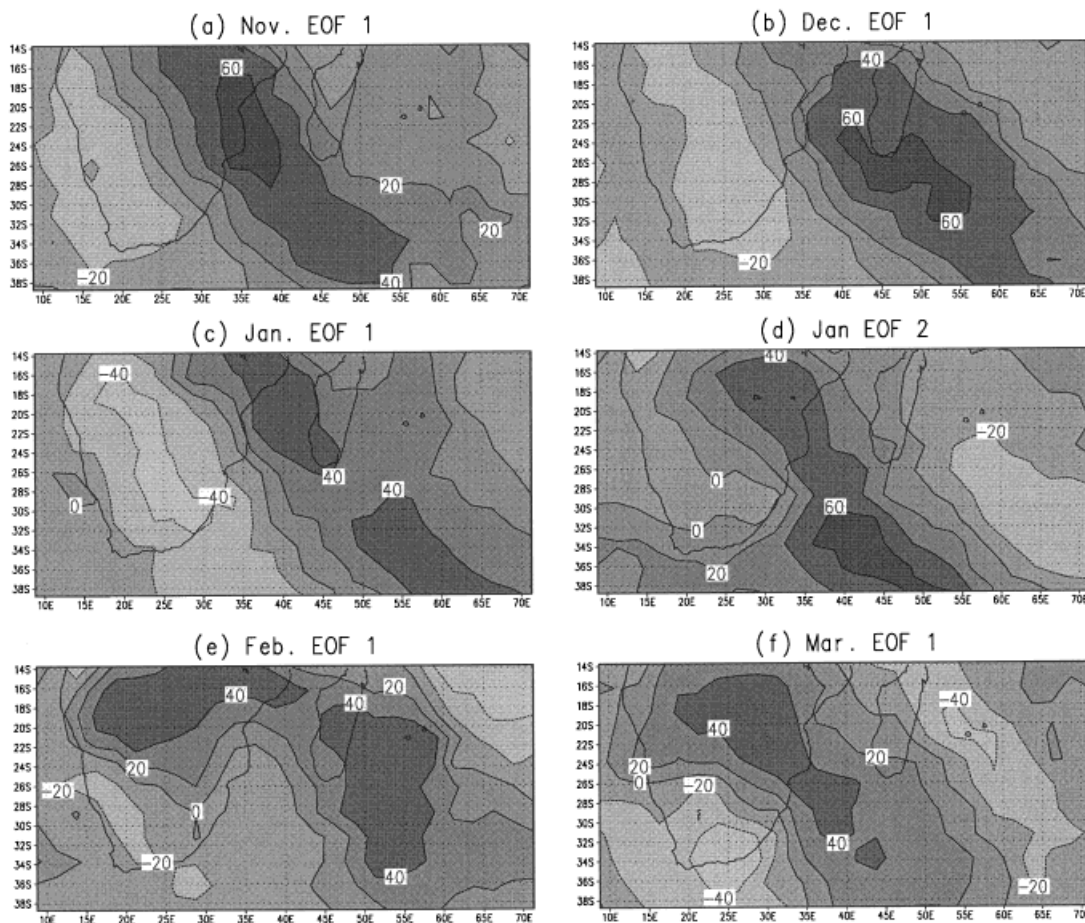


Figure 2. EOF weights of daily rainfall for: (a) November EOF1; (b) December EOF1; (c) January EOF1; (d) January EOF2; (e) February EOF1; (f) March EOF1

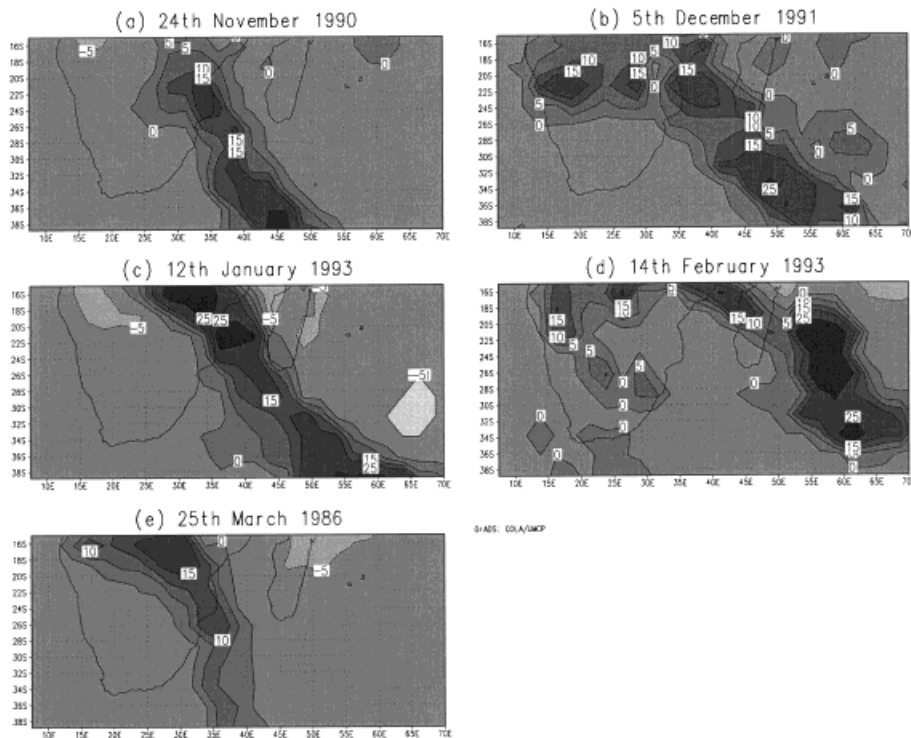


Figure 3. Daily rainfall anomalies in ( $\text{mm day}^{-1}$ ) associated with cases typical of the EOF loading patterns in each month

associated tropical–temperate link (Figure 2(e)). Rainfall over much of South Africa in February is not associated with this interaction.

Figure 3(d) shows an event typical of the February leading mode. In comparison with other case studies, this rainfall anomalies map shows positive anomalies across large parts of the domain, with peak values in the subtropical Southwest Indian Ocean.

March daily rainfall is organised in a dominant tropical–temperate band with the tropical component centred on Zimbabwe–Zambia and the temperate rainfall near  $35^{\circ}\text{S}$ ,  $40^{\circ}\text{E}$ . A weak and narrow band of negative loadings in the Southwest Indian Ocean parallels the dominant band (Figure 2(f)). An example of this EOF is given in Figure 3(e). Compared with previous months, the rainfall anomalies everywhere are weaker, and the tropical–temperate band of rainfall is narrower.

Next, the time coefficients of the leading EOFs (Figure 4) are discussed, which are computed as the cross product between the eigenvectors and the standardised rainfall time series. The time coefficients are useful in identifying daily rainfall events typical of each EOF. The frequency, longevity, and buildup of events is discussed. Since the months constituting the EOF are not time-continuous and since each of the monthly EOF patterns are different, spectra of the time coefficients are not meaningful and therefore have not been computed.

Important occurrences of tropical–temperate bands in November are limited to two events in 1991 and 1992, respectively, and single events in 1989 and 1990. The 1991 and 1992 events are of similar duration (3 days in 1991 and 2 days in 1992), separated by a 4–5-day period. Reversals from high-negative to high-positive coefficients between 7 and 16 November, 1991, suggest that the EOF has captured a propagating tropical–temperate band which entered or developed over the western half of southern Africa before propagating eastward. All the remaining events, which grow from low time coefficients, suggest stationary systems.

Events typical of the leading EOF pattern for December occur once in December 1991 and 1992, respectively, and twice in December 1986. Weak episodes are recorded in 1989 and 1990. Events are typically of 2–3 days in duration, with the exception of 1986, when an event sustained over 5–6 days occurred. The large events of 1991 and 1992 built suddenly, with the event in 1992 developing at the end of a month-long suppression of activity. Propagating bands, indicated by changes in sign in the EOF time coefficients, occurred between the 22 and 25 December, 1992 and also between 3 and 6 December, 1991, between the 15 and 20 December, 1990 and from 11–21 December, 1989.

Major January events occurred twice in 1993, once in 1986, 1987 and 1991, with sustained multiple episodes of moderate intensity throughout 1990 and 1992. The most intense events (highest time coefficients) had the characteristic of occurring 4 or 5 days apart (e.g. peaks at January 12, 1993 and January 20, 1993). Again, these peaks were short lived. Propagating system occurred on: 6–12 January, 1991; 19–26 January, 1987; 4–8 January, 1986; 10–12 January, 1993.

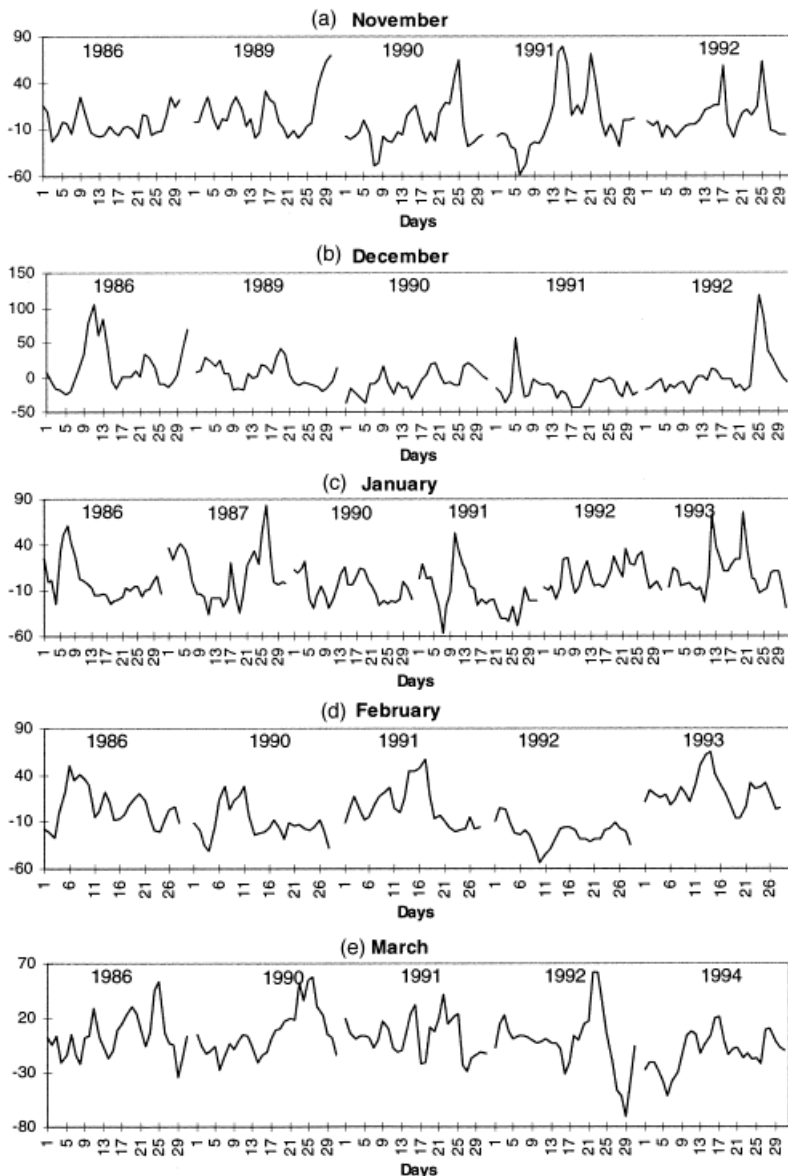


Figure 4. Time coefficients of EOFs: (a) November; (b) December; (c) January; (d) February; (e) March

Major February events occurred once in 1986, 1991 and 1993. A major negative event of suppressed rainfall was centred on 10 February, 1992, with a similar event of suppressed convection being the feature of early February 1990. Propagating systems are identifiable on 3–10 February 1986, 4–7 February 1990 and 10–15 February 1992.

During March, major episodes occurred once in 1992, 1990 and 1986. Episodes of suppressed convection occurred throughout 1994. Propagating systems are evident between 22 and 29 March 1992, between 6 and 13 March 1994, between 25 and 29 March 1986 and between 25 and 31 March 1990.

## 5. DISCUSSION

The structure of daily austral summer rainfall variability over southern Africa and the Southwest Indian Ocean has been analysed objectively for the first time. Tropical–temperate links are the main mode of daily rainfall variability in the region for each of the summer months November–March. These links are orientated north-west to south-east with a locus of activity over Zambia, Zimbabwe and Mozambique, extending to the Southwest Indian Ocean near 40°S and 50°E. In all months except February, these links have a dipole structure such that enhanced convection over the north-west to south-east-orientated band described above is associated with suppressed convection over a similarly orientated band with maxima over Namibia, South Africa and the Southern Ocean near 35°S and 30°E.

Identification of tropical–temperate rainfall links in southern Africa is based primarily on subjective analysis of daily satellite imagery and monthly rain gauge data (Harangozo and Harrison, 1983; Harrison, 1984a,b,c). Studies have argued that tropical temperate troughs (TTTs) form when a tropical low is coupled to a temperate westerly wave via a subtropical trough, forming a north-west to south-east cloud band along the leading edge of a westerly trough (Harangozo and Harrison, 1983; Harrison, 1984c; Tyson, 1986; Jury and Pathack, 1993). The tropical low locates over Southeast Angola or Southwest Zambia, forming preferentially during the period December–March at the furthest south-western limit of the ITCZ (Jury and Pathack, 1993). Tyson (1981) has shown that variations in mid-latitude pressure differences south-west and south-east of southern Africa, respectively, are in anti-phase with the rainfall oscillations over southern Africa. These adjustments are associated with the longitudinal position of the first ridge of wave 3 (Tyson, 1981). The structure of the leading mode of daily land and sea satellite rainfall variability captures both tropical and mid-latitude components of rainfall, which resemble features of variability derived from monthly data. While it is beyond the scope of this paper to demonstrate these links explicitly, it seems reasonable that the monthly patterns of atmospheric variability described by Tyson (1981), Harangozo and Harrison (1983), Harrison (1984a,b,c), Tyson (1986), Jury and Pathack (1993) and others, have their origin, at least in part, in the types of synoptic systems captured in these leading EOFs of daily rainfall.

An important feature of the daily rainfall EOFs is a dipole structure with centres separated by some 25–30° of longitude. In all months except February, the dipole occurs as a parallel band from north-west to south-east extending over at least 30° of latitude. The nature of a rainfall dipole has also been examined by Tyson (1986), Jury (1992), Jury and Pathack (1993), Jury and Pathack (in press) and Jury *et al.* (1994), again on the basis of monthly data. Dry summer months over southern Africa are dominated by confluent upper winds, which reduce the potential for convection over southern Africa. Contemporaneously, tropical disturbances are enhanced in the Southwest Indian Ocean, representing an eastward shift in the preferred location of summer convection (Harangozo and Harrison, 1983; Jury and Pathack, 1991, 1993; Jury *et al.*, 1992, 1994; Jury 1996). Changes in OLR (Jury and Walliser, 1990; Jury *et al.*, 1992) confirm that decreases in convection over the subcontinent during dry years are often compensated by increases to the east of Madagascar with weakened divergence of moisture from the equatorial Indian Ocean during dry years (D'Abreton and Lindesay, 1993; D'Abreton and Tyson, 1995). Interactions between the stratospheric QBO and the Walker Circulation over south-eastern southern Africa are thought to induce strong upper tropospheric westerlies off the east coast of southern Africa during the westerly phase of the QBO. This is associated with convection and upper-level divergence over southern Africa (Jury, 1992; Jury and Pathack, 1993; Jury *et al.*, 1994).

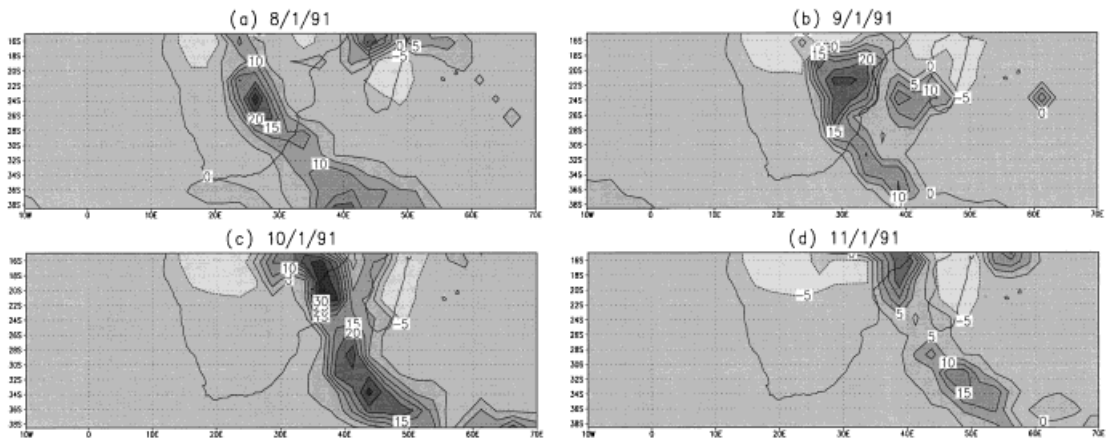


Figure 5. Daily rainfall anomalies ( $\text{mm day}^{-1}$ ) associated with a propagating system 8–11 January 1991

What is clear from this study is that the rainfall dipole originates in specific synoptic episodes which occur relatively infrequently, but emerge as clear signals in the monthly anomaly fields. Furthermore, the dipole is realised as tropical–temperate links over both southern Africa and the Southwest Indian Ocean. Studies of the dipole which use land-based rain gauge data (Jury *et al.*, 1992) as the sampling basis have only considered the tropical component of this tropical–temperate feature.

Shinoda and Kawamura (1986), Jury (1992), Jury *et al.* (1994) and Stokes *et al.* (1997) have all produced evidence suggesting the reversal of a Walker cell over the east coast and south-western Indian Ocean between wet and dry years as a mechanism for the convective dipole. Given that the modes of daily rainfall variability have been shown to have propagating components, the timescales of the adjustments to the Walker Cell in the Southwest Indian Ocean can be remarkably short, certainly occurring on synoptic timescales associated with tropical–temperate links. Figures 5–7 show examples of propagating systems, identifiable of the EOF time coefficients as marked changes in sign (Figure 4), which amount to short term rearrangement of the local Walker Cell. The sequence from 8 to 11 January 1991 (Figure 5)

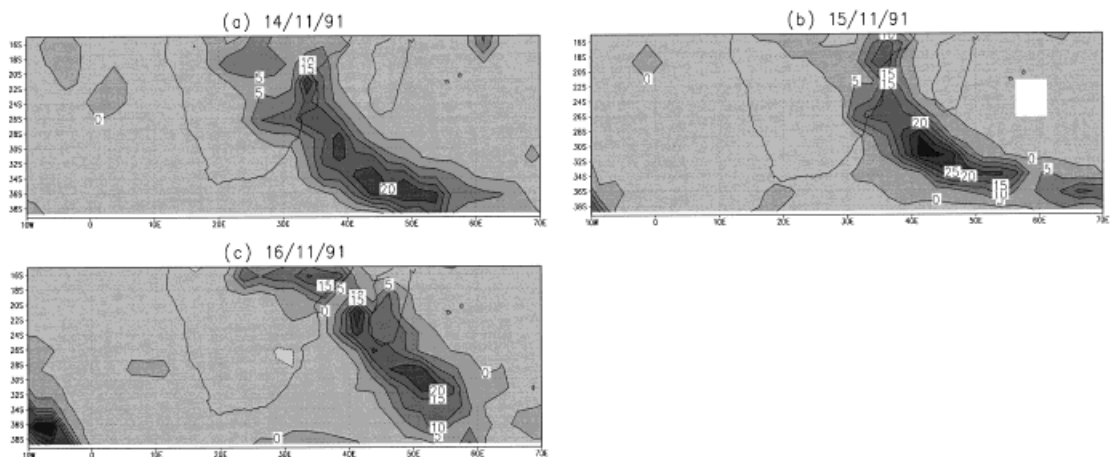


Figure 6. Daily rainfall anomalies ( $\text{mm day}^{-1}$ ) associated with a propagating system 14–16 November 1991

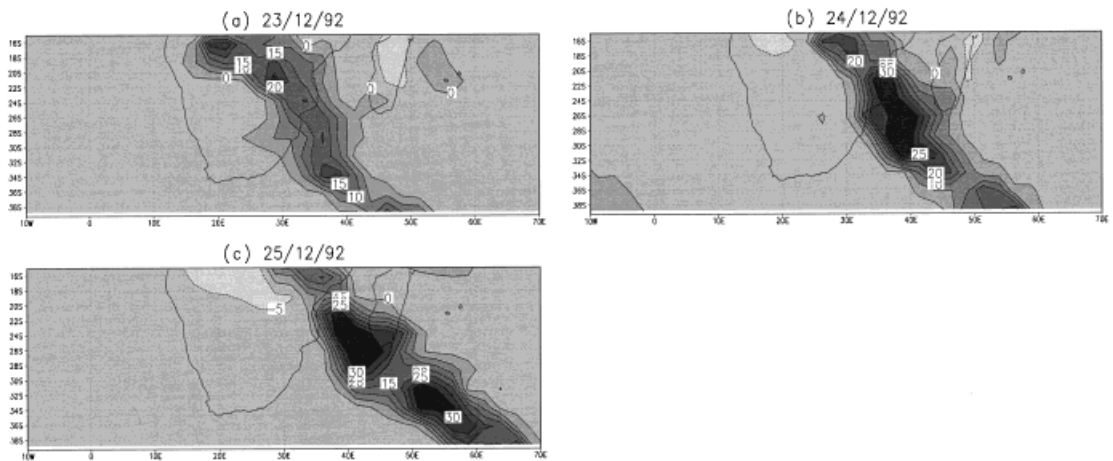


Figure 7. Daily rainfall anomalies ( $\text{mm day}^{-1}$ ) associated with a propagating system 23–25 December 1992

shows the growth and eastward propagation of a TTT. During this time, the western edge of the TTT migrates from 20 to 35°E while the rainfall rate builds to peak on 10 January. Examples of early summer propagation are shown in Figure 6. Between 14 and 16 November 1991, the TTT moves off the eastern coast of southern Africa and centres over southern Madagascar. The highest rainfall rates again occur whilst the TTT is located between the subcontinent and Madagascar. Figure 7 shows the propagation during December (23–25 December 1992). During these episodes, rainfall anomalies of  $> 25 \text{ mm day}^{-1}$  are to be found in the tropical and temperate components of the rain-band.

Adjustments to the local Walker circulation have also been invoked on much longer timescales to explain aridity episodes during the Quaternary (Stokes *et al.*, 1997), the climate of the last glacial maximum (Cockcroft *et al.*, 1987) and the recent Holocene (Tyson and Lindesay, 1992). Recognition of the dipole on daily timescales may provide insights into the nature of climate change, since systems responsible for day to day variability in rainfall may also be responsible for adjustments over millennia. Such suggestions require rigorous tests and are the subject of on going research.

Given the short duration of the data, a full analysis of the frequency of TTTs cannot be made. Figure 8 shows the mean modulus of the monthly leading EOF time coefficients for each of the years studied. High values indicate intense and/or frequent activity. The interannual variability of the synoptic activity is pronounced, particularly in early summer, where the range of coefficients is about 100% between inactive and active years. This variability decreases somewhat in February and March.

Some caution nevertheless needs to be attached to the interpretation of these results owing to the relatively short duration of the data set. Within the context of EOF analysis, the input matrix of observations (daily rainfall in this case) ranges from 144 to 186 and is reasonable, given that interannual rainfall variability is often studied using 50 observations (corresponding to 50 or so years available). But within the context of rainfall systems associated with the leading EOFs, the record is short, since the rainfall events occur infrequently, often only once or twice per month. While it is remarkable that such infrequent events still impose a signal which emerges as the leading EOF, caution must nevertheless be attached to the discussion surrounding the location of the tropical–temperate troughs. The location of the trough axis may be sensitive to the incorporation of additional data. This sensitivity could be addressed using Monte Carlo methods whereby the trough axis position is mapped for each leading EOF, following random exclusion of observations over many iterations, but it is probably prudent to await more data, given the computer time involved in such approaches.

More importantly, the years studied here include a preponderance of Pacific warm episodes, largely as a result of the prolonged El Niño of the early 1990s. Obviously a larger sample of cold events would

afford wider interpretation of these results, although such cold events have been infrequent over the last few decades. For this reason caution should again be attached to the location of the tropical-temperate links.

The EOFs discussed in this paper have been confined to the leading mode for each month. This approach has allowed discussion of the main modes of cloud bands, but not all the cloud bands. Using January as an example, bands on the 19.1.86, 21.1.86, 26.1.86 and 27.1.86 are all readily identifiable on daily maps of rainfall anomalies, but do not appear on January EOF1 time coefficients (Figure 3). If the

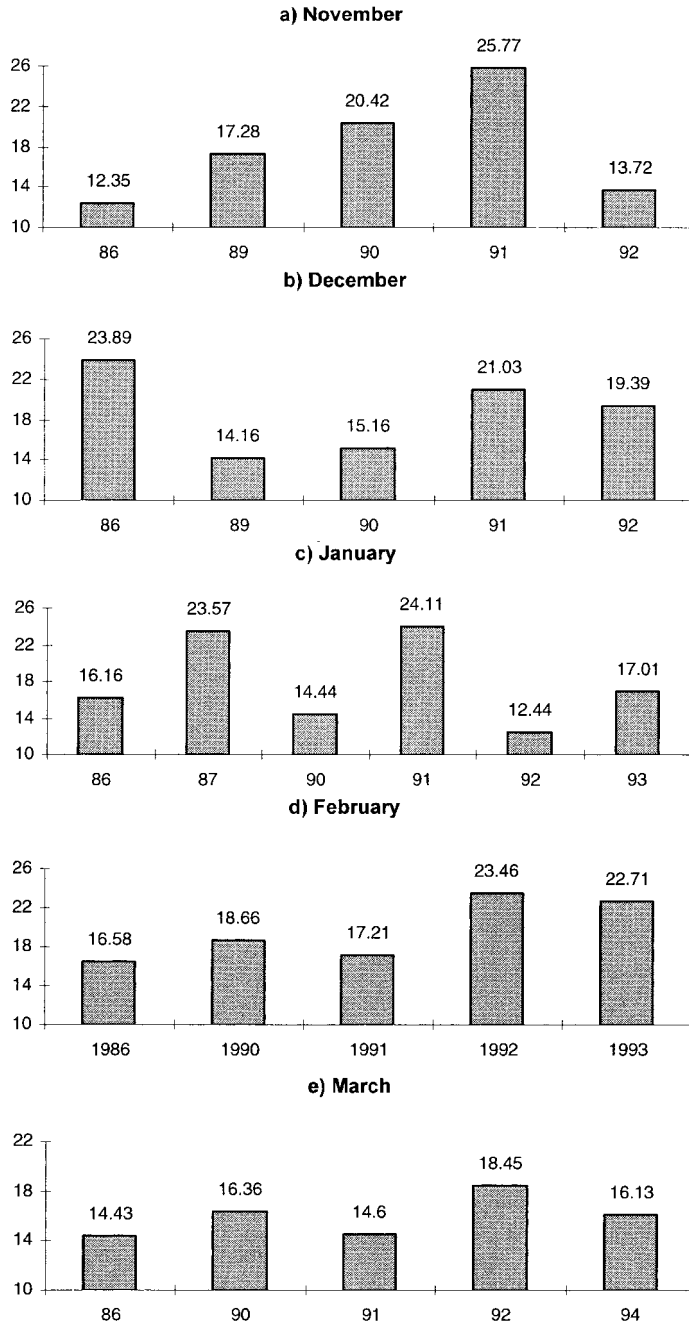


Figure 8. Mean monthly modulus of EOF time coefficients for each of the study years

EOF domain is reduced to land areas only, these bands do appear in the leading EOF. Likewise, Jury (1997) has noted that in the absence of a midlatitude links, truncated troughs often form over southern Africa. These may be more common than tropical–temperate troughs. While a complete analysis of rainfall modes is beyond the aims of this paper, the important result that has emerged, is that centres of rainfall variability do not occur over South Africa. Analysis of rainfall from rain gauge data may have led to inflated attention being given to the importance of the atmospheric circulation variability of South Africa, rather than the Southwest Indian Ocean, where EOF loadings are highest.

## 6. CONCLUSIONS

This work presents the first objective analysis of land- and ocean-based daily rainfall variability in the southern African–Southwest Indian Ocean region. In all months (November–March), the leading mode of daily rainfall variability is a tropical–temperate link spanning the latitudinal domain of the study. With the exception of February, these links have a parallel structure, such that enhanced (suppressed) activity in bands off the east coast of Africa are associated with suppressed (enhanced) activity over southern Africa. Previous studies based on rain gauge data have used southern Africa as a sampling base, thereby emphasising the importance of land-based subtropical rainfall. This study has shown that the centre of variability lies offshore in the Southwest Indian Ocean and not over the southern African land-mass.

Similarity in structure between rainfall dipoles analysed on the basis of monthly data (Jury, 1992) and the analysis of daily satellite-derived rainfall, suggests that individual synoptic events are likely to be responsible for interannual variability in southern African rainfall. Southern Africa and the surrounding Southwest Indian Ocean emerges as an important setting for tropical–temperate interaction on daily timescales. Although both the northern and southern subtropics of Africa have a marked degree of decadal rainfall variability (Tyson, 1986; Ward, 1995), southern Africa is distinct from its northern subtropical counterpart in the degree of linkage between tropical and temperate rainfall systems. It remains to determine whether decadal rainfall variability can also be linked to specific synoptic systems. Such work is being undertaken by means of century-long integrations of GCMs.

## ACKNOWLEDGEMENTS

The authors are grateful to the University of Oxford for funding. The ISCCP satellite data were obtained from the NASA Langley Research Centre, EOSDIS, Distributed Active Archive Centre. RW gratefully acknowledges support from DOE contract # -PECD/7/12/37 and for helpful discussions with Chris Folland. Thanks also to Brad Delp and Tom Scholz.

## REFERENCES

- Arkin, P.A. and Meisner, B.N. 1987. 'The relationship between large-scale convective rainfall and cold cloud over the western hemisphere during 1982–82', *Monthly Weather Review*, **115**, 51–74.
- Arkin, P.A., Joyce, R. and Janowiak, J.E. 1994. 'The estimation of global monthly mean rainfall using infrared satellite data: the GOES Precipitation Index (GPI)', *Remote Sensing Reviews*, **11**(1–4), 107–124.
- Barrett, E.C. and Beaumont, M.J. 1994. 'Satellite rainfall monitoring: an overview', *Remote sensing Reviews*, **11**(1–4), 49–60.
- Buell, C.E. 1975. 'The topography of the empirical orthogonal functions', in Fourth Conference on Probability and Statistics in Atmospheric Sciences, Tallahassee, American Meteorological Society.
- Cockcroft, M.J., Wilkinson, M.J. and Tyson, P.D. 1987. 'The application of a present-day climatic model to the late Quaternary in southern Africa', *Climatic Change*, **10**, 161–181.
- Cohen, A.L. and Tyson, P.D. 1995. 'Sea-surface temperature fluctuations during the Holocene off the south coast of Africa: implications for terrestrial climate and rainfall', *The Holocene*, **5**(3), 304–312.
- D'Abreton, P.C. and Lindsay, J.A. 1993. 'Water vapour transport over southern Africa during wet and dry early and late summer months', *Int. J. Climatol.*, **13**, 151–170.
- D'Abreton, P.C. and Tyson, P.D. 1995. 'Divergent and non-divergent water vapour transport over southern Africa during wet and dry conditions', *Meteorol. Atmos. Phys.*, **55**, 47–59.
- Diab, R.D., Preston-Whyte, R.A. and Washington, R. 1991. 'Distribution of rainfall by synoptic type over Natal, South Africa', *Int. J. Climatol.*, **11**, 877–888.

- Folland, C.K., Parker, D., Colman, A. and Washington, R. (in press). 'Low frequency variability of worldwide ocean surface temperature in the historical record', in Navarra, A (ed.), *Beyond El Niño: Decadal Variability in the Climate System* Springer-Verlag, 24 p.
- Harangozo, S. and Harrison, M.S.J. 1983. 'On the use of synoptic data indicating the presence of cloud bands over southern Africa', *S. Afr. J. Sci.*, **79**, 413.
- Harrison, M.S.J. 1984a. 'A generalised classification of South African summer rain-bearing synoptic systems', *J. Climatol.*, **4**, 547–560.
- Harrison, M.S.J. 1984b. 'The annual rainfall cycle over the central interior of South Africa', *S. Afr. Geogr. J.*, **66**, 46–47.
- Harrison, M.S.J. 1984c. 'Comparison of rainfall time series over South Africa generated through real data and through principal component analysis', *J. Climatol.*, **4**, 561–564.
- Huffman, G.J., Adler, R.F., Arkin, P., Chang, A., Ferraro, R., Gruber, A., Janowiak, J., McNab, A., Rudolf, B. and Schneider, U. 1997. 'The Global Precipitation Climatology Project (GPCP) combined precipitation dataset', *Bull. Am. Meteorol. Soc.*, **78**, 5–20.
- Janowiak, J.E. and Arkin, P.A. 1991. 'Rainfall variation in the tropics during 1986–1989, as estimated from observation of cloud-top temperature', *J. Geophys. Res.*, **96**, supplement, 3359–3373.
- Joliffe, I.T. 1987. 'Rotation of principal components: some comments', *J. Climatol.*, **7**, 507–510.
- Joyce, R. and Arkin, P.A. 1997. 'Improved estimates of tropical and subtropical precipitation using the GOES Precipitation Index (GPI)', *J. Atmos. Oceanic Technol.*, **14**, 997–1011.
- Jury, M.R. 1992. 'A climatic dipole governing the interannual variability of convection over the SW Indian Ocean and SE Africa region', *Trends Geophys. Res.*, **1**, 165–172.
- Jury, M.R. 1996. 'Regional teleconnection patterns associated with summer rainfall over South Africa, Namibia and Zimbabwe', *Int. J. Climatol.*, **16**, 135–153.
- Jury, M.R. 1997. 'Interannual climate modes over southern Africa from satellite cloud OLR 1975–1994', *Theor. Appl. Climatol.*, **57**, 155–163.
- Jury, M.R. and Walliser, D. 1990. 'Satellite microwave measurements of atmospheric water vapour and marine windspeed, case study application', *S. Afr. J. Marine Sci.*, **9**, 309–316.
- Jury, M.R. and Pathack, B.M.R. 1991. 'A study of climate and weather variability over the tropical SW Indian Ocean', *Meteorol. Atmos. Phys.*, **47**, 37–48.
- Jury, M.R., Pathack, B.M.R. and Sohn, B.J. 1992. 'Spatial structure and interannual variability of summer convection over southern Africa and the SW Indian Ocean', *S. Afr. J. Sci.*, **88**, 275–280.
- Jury, M.R. and Pathack, B.M.R. 1993. 'Composite climatic patterns associated with the 1992 drought over southern Africa: 1975–1984', *Theor. Appl. Climatol.*, **47**, 137–145.
- Jury, M.R. and Pathack, B.M.R. (in press). 'Climatic patterns associated with the 1992 drought over southern Africa: observations and GCM results', *J. Afr. Meteorol. Soc.*
- Jury, M.R., McQueen, C.A. and Levey, K.M. 1994. 'SOI and QBO signals in the African region', *Theor. Appl. Climatol.*, **50**, 103–115.
- Kidd, C. and Adler, R.F. 1997. 'Global satellite rainfall estimation: results of the Third Precipitation Intercomparison Project', *Proceedings of the Twenty-Third Conference of the Remote Sensing Society*, Reading, U.K., Remote Sensing Society, pp. 481–486.
- Li, Q., Bras, R.L. and Veneziano, D. 1996. 'Analysis of Darwin rainfall data: Implications on sampling strategy', *J. Appl. Meteorol.*, **35**, 372–385.
- Lindesay, J.A. and Jury, M.R. 1991. 'Atmospheric circulation controls and characteristics of a flood event in central South Africa', *Int. J. Climatol.*, **11**, 609–627.
- Morrissey, M.L. and Janowiak, J.E. 1996. 'Sampling-induced conditional biases in satellite climate-scale rainfall estimates', *J. Appl. Meteorol.*, **35**, 541–548.
- Nogues-Paegle, J. and Mo, K.C. 1997. 'Alternating wet and dry conditions over South America during summer', *Monthly Weather Review*, **125**, 279–291.
- North, G.R., Bell, T.L., Cahalan, R.F. and Moeng, F.J. 1982. 'Sampling errors in the estimation of empirical orthogonal functions', *Monthly Weather Review*, **110**, 699–706.
- Richman, M.B. 1986. 'Rotation of principal components', *Int. J. Climatol.*, **6**, 293–335.
- Rossow, W.B. and Schiffer, R.A. 1991. 'ISCCP cloud data products', *Bull. Am. Meteorol. Soc.*, **72**, 2–20.
- Rossow, W.B., Walker, A.W., Beusichel, D.E. and Roiter, M.D. 1996. *ISCCP: Documentation of New Cloud Datasets*, WMO-TD, World Climate Research Programme (ICSU and WMO), Geneva, 115 pp.
- Schiffer, R.A. and Rossow, W.B. 1985. 'ISCCP global radiance data set: A new resource for climate research', *Bull. Am. Meteorol. Soc.*, **66**, 1498–1505.
- Shinoda, M. and Kawamura, R. 1986. 'Relationships between rainfall over semi-arid southern Africa and geopotential heights and sea surface temperatures', *J. Meteorol. Soc. Jpn.*, **74**, 21–36.
- Soman, V.V., Valdes, J.B. and North, G. 1995. 'Satellite sampling and the diurnal cycle statistics of Darwin rainfall data', *J. Appl. Meteorol.*, **34**, 2481–2490.
- Smith, A.V. 1985. 'Studies of the effects of cold fronts during rainy season weather in Zimbabwe', *Weather*, **40**, 198–203.
- Stokes, S., Thomas, D.S.G. and Washington, R. 1997. 'Multiple episodes of aridity in southern Africa since the last interglacial', *Nature*, **388**(6638), 154–158.
- Todd, M. and Washington, R. 1998. 'A simple method to retrieve 3-hourly estimates of global tropical and subtropical precipitation from International Satellite Cloud Climatology Program (ISCCP) D1 data', *J. Atmos. Oceanic Technol.* (in press).
- Tyson, P.D. 1981. 'Atmospheric circulation variations and the occurrence of extended wet and dry spells over southern Africa', *J. Climatol.*, **1**, 115–130.
- Tyson, P.D. 1986. *Climatic Change and Variability in Southern Africa*, Oxford University Press, Cape Town.
- Tyson, P.D. 1993. 'Recent developments in the modelling of the future climate of southern Africa', *S. Afr. J. Sci.*, **89**, 494–505.
- Tyson, P.D. and Lindesay, J.A. 1992. 'The climate of the last 2000 years in southern Africa', *The Holocene*, **2**(3), 271–278.

- Walker, N.D. and Lindsay, J.A. 1989. 'Preliminary observations of oceanic influences on the February–March 1988 floods in central South Africa', *Int. J. Climatol.*, **11**, 609–627.
- Ward, M.N. 1995. 'Analysing the boreal summer relationship between world-wide sea surface temperatures and atmospheric variability', in von Storch, H. and Navarra, A. (eds), *Analysis of Climate Variability*, Springer.
- White, D., Richman M. and Yarnal, B. 1991. 'Climate regionalisation and rotation of principal components', *Int. J. Climatol.*, **11**, 1–25.
- Xie, P. and Arkin, P.A. 1997. 'Analysis of global monthly precipitation using gauge observations, satellite estimates and numerical model predictions', *J. Clim.*, **9**, 840–858.